Bench-scale photoelectrocatalytic reactor utilizing rGO-TiO2 photoanodes for the degradation of contaminants of emerging concern in water

Alkharabsheh, S., McMichael, S., Singhal, A., Rioja-Cabanillas, A., Zamora, P., Monsalvo, V., Rogalla, F., Byrne, J. A., & Fernández-Ibáñez, P. (2024). Bench-scale photoelectrocatalytic reactor utilizing rGO-TiO2 photoanodes for the degradation of contaminants of emerging concern in water. *Process Safety and Environmental Protection*, *182*, 833-844. Advance online publication. https://doi.org/10.1016/j.psep.2023.12.009

Link to publication record in Ulster University Research Portal

Published in:
Process Safety and Environmental Protection

Publication Status:
Published online: 29/02/2024

DOI:
10.1016/j.psep.2023.12.009

Document Version
Publisher's PDF, also known as Version of record

General rights
Copyright for the publications made accessible via Ulster University's Research Portal is retained by the author(s) and / or other copyright owners and it is a condition of accessing these publications that users recognise and abide by the legal requirements associated with these rights.

Take down policy
The Research Portal is Ulster University's institutional repository that provides access to Ulster's research outputs. Every effort has been made to ensure that content in the Research Portal does not infringe any person's rights, or applicable UK laws. If you discover content in the Research Portal that you believe breaches copyright or violates any law, please contact pure-support@ulster.ac.uk.

Download date: 12/01/2024

Process Safety and Environmental Protection 182 (2024) 833–844

Contents lists available at ScienceDirect

Process Safety and Environmental Protection

journal homepage: www.journals.elsevier.com/process-safety-and-environmental-protection

Bench-scale photoelectrocatalytic reactor utilizing rGO-TiO_2 photoanodes for the degradation of contaminants of emerging concern in water

S. Alkharabsheh [a,*], S. McMichael [a], A. Singhal [a], A. Rioja-Cabanillas [a], P. Zamora [b], V. Monsalvo [b], F. Rogalla [b], J.A. Byrne [a], P. Fernández-Ibáñez [a,*]

[a] Nanotechnology and Integrated BioEngineering Centre, Ulster University, Belfast BT15 1AP, United Kingdom
[b] FCC Aqualia, Avenida Camino de Santiago 40, Building 3, 4th floor, Madrid 25080, Spain

ARTICLE INFO

Keywords:
Photoelectrocatalysis
RGO
TiO_2
UVA-LED reactor
Diclofenac

ABSTRACT

Pharmaceuticals and personal care products are contaminants of emerging concern (CEC) in water. Photocatalysis (PC) and photoelectrocatalysis (PEC) are potential advanced oxidation processes for the effective degradation of these contaminants. In this work a bench-scale photoelectrocatalytic reactor utilizing a UVA-LED array was designed and tested for the degradation of diclofenac as a model CEC. Reduced graphene oxide-titanium dioxide (rGO-TiO_2) composite, prepared by the photocatalytic reduction of rGO on TiO_2, was immobilised on fluorine doped tin oxide (FTO) glass and evaluated as a photoanode. The influence of UVA intensity and rGO:TiO_2 ratio on the degradation rate was studied. Surface modification of the TiO_2 with 1% rGO gave the highest photocurrent and best degradation rate of diclofenac, as compared to unmodified TiO_2. However, following repeat cycles of photoelectrocatalytic treatment there was an observed drop in the photocurrent with rGO-TiO_2 anodes and the rate of diclofenac degradation decreased. Raman and XPS analysis indicated the re-oxidation of the rGO. Attempts to regenerate the rGO in-situ by electrochemical reduction did not prove successful, suggesting that the site of photoelectrocatalytic oxidation of rGO was different to the reduction site targeted in the photocatalytic reduction for the formation of the rGO-TiO_2 composites.

1. Introduction

PEC (photoelectrocatalysis) has been widely researched as a novel technology with the potential to remove organic pollutants and harmful microorganisms from water and wastewater (Kusmierek, 2020). The advantages of PEC include environmental friendliness, effective degradation of CEC, and improved performance compared to PC alone due to enhanced charge carrier separation by the applied potential (Daghrir et al., 2012; Alulema-Pullupaxi et al., 2021). PEC is commonly conducted using an n-type photoanode with a metallic or carbon counter electrode connected by an external circuit in an electrochemical cell. The photoanode can be excited by irradiation with energy that is equal to or greater than the bandgap energy of the material, the excitation produces an electron-hole pair (e^--h^+). The applied potential generates an electric field and promotes the transfer of photogenerated electrons to counter electrode through an external circuit, reducing charge carrier recombination and improving process efficiency. The photogenerated holes can either directly oxidize organic pollutants or react with the absorbed water to produce hydroxyl radicals ($HO^\bullet$). The electrons at the cathode can reduce oxygen and generate superoxide radicals ($O_2^{\bullet-}$) which undergo subsequent reactions forming other reactive oxidizing species (ROS), such as hydrogen peroxide (H_2O_2), hydroperoxyl radical $HO_2^\bullet$, and $HO^\bullet$. The ROS attack and degrade organic pollutants, eventually to H_2O and CO_2 (Fernandez-Ibanez et al., 2021; McMichael et al., 2021).

Several different photoelectrochemical reactors have been tested such as rotating disk, thin film and cylindrical PEC have been reported in the literature (McMichael et al., 2021). However, these designs remain restricted to the laboratory scale and have various limitations, including a lack of adequate homogeneous irradiation sources, low mass transfer, energy loss during irradiation, complex electrode preparation, and PEC cell maintenance limitations (Meng et al., 2015, Wang et al., 2020, McMichael et al., 2021). In addition, other challenges during the design of PEC reactors must be addressed, including the fabrication of photoanodes that allow back-face irradiation, and cell design to minimise electrical resistant and give a high electrode surface area-to-volume ratio (Meng et al., 2015; McMichael et al., 2021, 2022). Several

* Corresponding authors.
E-mail addresses: Alkharabsheh-s@ulster.ac.uk (S. Alkharabsheh), p.fernandez@ulster.ac.uk (P. Fernández-Ibáñez).

https://doi.org/10.1016/j.psep.2023.12.009
Received 16 October 2023; Received in revised form 23 November 2023; Accepted 4 December 2023
Available online 21 December 2023
0957-5820/Crown Copyright © 2023 Published by Elsevier Ltd on behalf of Institution of Chemical Engineers. This is an open access article under the CC BY license (http://creativecommons.org/licenses/by/4.0/).

irradiation sources have been tested in PEC systems including mercury, xenon, and halogen lamps (Wang et al., 2020). However, each of these sources is associated with limitations such as fragility, excessive heat generation, high energy consumption, environmental risk, short life span, and unhomogenized irradiation in the reactor (Song et al., 2016; Martín-Sómer et al., 2017, Wang et al., 2020). Considering these issues, light-emitting diode (LED)–based lamps with controllable, high-intensity, and uniform irradiance are promising for PEC applications (Song et al., 2016, Wang et al., 2020).

Titanium dioxide (TiO_2) particulate electrodes formed by the immobilization of TiO_2 particles on a conducting support have been employed as photoanodes. The photocurrent is normally quite low due to the requirement of photogenerated electrons to pass between particle boundaries to reach the supporting electrode, and surface recombination reactions will predominate in the absence of hole scavengers. One approach to improve electron transport to the supporting electrode is to introduce a conducting element such as graphene into the TiO_2 layer.

Graphene-based materials have been widely employed in designing novel photocatalysts due to their advantageous physical properties, including unique optical properties, large specific surface area, excellent mechanical strength, and high electronic conductivity. TiO_2-based composites made with graphene and reduced graphene oxide (rGO) have emerged as promising materials for PC and PEC (D. Wang et al., 2012; P. Wang et al., 2012, Cruz-Ortiz, 2017). rGO-TiO_2 composites have been demonstrated to exhibit improved photocatalytic efficiency due to several different mechanisms including efficient charge transport, reduced electron-hole recombination rates, prolonged carrier lifetime, altered ROS distribution (Wang et al., 2012; Cruz-Ortiz et al., 2017), and excellent pollutant adsorption (Low et al., 2017). Commonly, rGO is prepared by reducing graphene oxide (GO) using thermal or chemical reduction methods (Cruz-Ortiz et al., 2017). However, functional oxygen groups may not be completely removed in the reduction stage, and the reduced form is referred to as reduced graphene oxide (rGO). Owing to the noted properties, rGO-TiO_2 composites have been widely employed as photocatalysts for water disinfection and organic pollutant removal such as *E.coli* (Cruz-Ortiz et al., 2017), *K. pneumoniae*, *E. faecium & B. bacteriovorus* (Waso et al., 2020), phenol (Naknikham et al., 2019), bisphenol (Žerjav et al., 2017), clofibric acid (Tolosana-Moranchel et al., 2019a and 2019b), diphenhydramine, and methyl orange (Pastrana-Martínez et al., 2012). Pastrana-Martínez et al. (2012) reported improvement in the photocatalytic activity of TiO_2 when combined with rGO, demonstrating total degradation and significant mineralization of diphenhydramine and methyl orange in less than 60 min under near UV-Vis irradiation (Pastrana-Martínez et al., 2012). However, these studies did not show whether the nanocomposites and their photocatalytic activity remain stable after the photocatalytic process. Taking into consideration that TiO_2 is activated by UV irradiation and ROS, which are highly oxidative and can degrade organic pollutants, therefore oxidation reactions with rGO cannot be discarded. Furthermore, the effect of irradiation on the rGO structure and the stability during PC and PEC processes has not been completely elucidated up to now.

This work evaluates rGO-TiO_2 composite photoanodes prepared by photocatalytic reduction of GO for the photoelectrolytic degradation of diclofenac in a bench scale photoelectrochemical reactor irradiated with a controllable high-intensity UVA-LED array. The stability of the rGO-TiO_2 photoanodes was investigated by repeat cycles of treatment and surface characterisation post treatment.

2. Experimental

2.1. Materials and reagents

Diclofenac sodium (>99%) and sodium sulfate (Na_2SO_4) (>99%) were obtained from Acros Organics. Methanol anhydrous was obtained from Scharlab (99.9%), Degussa P25 TiO_2 was obtained from Aeroxide, graphene oxide (GO) was obtained from Versarien PLC, deacon 90 detergent was obtained from Deacon Laboratories, and platinized titanium (Pt/Ti) was obtained from Umicore. All solutions were prepared with distilled water obtained from a laboratory water purification system.

2.2. rGO-TiO_2 composite synthesis

The rGO-TiO_2 composite was synthesized by photocatalytic reduction method. In which GO and TiO_2 particles were suspended separately in 50 mL of methanol and sonicated using the Elmasonic P60H ultrasonic instrument for 1 h. The two suspensions were mixed to obtain a concentration of 1 or 5 wt% GO/TiO_2. The resulting suspension was sonicated for 1 h and then irradiated with 14.4 $mWcm^{-2}$ UVA-LED for 5 h to reduce the GO and form the rGO-TiO_2 composite, the resulting solution was then evaporated in air with the rGO-TiO_2 nanopowder remaining (Cruz-Ortiz et al., 2017).

2.3. Photoanode preparation

FTO glass (23 cm × 29.5 cm) was cleaned using 5% deacon90 detergent, followed by multiple rinses with distilled water. Subsequently, the cleaned FTO substrate was left to dry in air. The FTO substrate was spray-coated using an airbrush spray gun. A methanol solution containing 1% w/v of the required material (Degussa P25 TiO2, 1% rGO-TiO2, or 5% rGO-TiO2), which had been sonicated for 15 min before usage, was applied as coating solution. The FTO was coated until the optimal catalyst loading of 1 $mgcm^{-2}$ was achieved as reported in the literature (Byrne et al., 1998b; Dunlop et al., 2010). The FTO substrate was weighed before and after spray coating, with the coating process continuing until a weight increase of 0.65 g was attained, signifying the achievement of optimal loading. The coated electrodes were then annealed at 450 °C for 2 h to facilitate adhesion. To carry out surface characterization, all samples were prepared using the same method as the large photoanode and sprayed onto 1 cm × 1 cm FTO excluding the GO sample, which was not annealed.

2.4. Materials characterization

Visual changes were examined and confirmed the successful reduction of GO. A field emission scanning electron microscope (FESEM) was used to analyze the surface morphology of the prepared electrodes, using FESEM SU5000 (Hitachi) operated under high vacuum conditions of $\sim 10^{-8}$ bar. The FESEM was equipped with a dispersive energy X-ray (EDX/EDS) analyzer, which was used to determine the bulk elemental composition. Composition analyses were conducted at an accelerating voltage of 7.5 kV. EDX images were recorded using a backscattered secondary electron detector and analyzed using the Aztec software provided with the instrument. EDX was used to confirm rGO presence by examining carbon percentage in the TiO_2 sample. A Renishaw Raman spectroscopy was used to evaluate the crystal structure of the samples at room temperature with 532 nm argon neon laser sources. For each sample, the scan was recorded 3 times with an exposure period of 10 s in the range of 3200 – 1000 $cm^{-1.}$

Chemical composition analysis was carried out by X-ray photoelectron spectroscopy (XPS) using a Kratos Axis Ultra employing an Al Kα X-ray source ($h\nu$ 1486.7 eV). Wide energy survey scans were performed for samples at a binding energy range of 0 – 1250 eV with 150 kV pass energy. High-resolution scans were performed at a slower scan speed for specific elemental transitions at 20 kV pass energy. For charge correction, the binding energy of the samples was calibrated relative to the C 1 s peak at 284 eV (Fernández-Ibáñez et al., 2015). The XPS spectra were analyzed using Advantage software. The quantification peaks were fitted using a mixed Gaussian–Lorentzian function after performing a smart background correction. All scans were performed at a minimum of three sites to reduce errors in determining elemental proportions.

2.5. Photoelectrocatalytic reactor

The reactor (Fig. 1) was designed based on a sandwich type configuration with the photoanode flat plate electrode directly opposite and in-parallel to the counter electrode to minimise resistance losses. A fluid channel was used to increase the residence time. The photoanodes were fabricated using FTO as the supporting electrode to allow back-faced irradiation was used to ensure photon absorption by the photocatalyst and not by the electrolyte solution (McMichael et al., 2021). The interior volume of the channel's reactor was 450 mL. The FTO glass was used as the conductive support for the photoanode (23 cm × 29.5 cm) and had a geometric surface area of 534.6 cm^2 (19.8 cm × 27 cm) when placed in the reactor. The height of the channels was 0.8 mm and located at distance of 0.2 cm far from the FTO glass. The cathode was platinized titanium plate (2 mm thick), which was machined to fit the shape of the channels. The distance between the working and counter electrodes was 0.8 cm. The irradiation source comprised of four CL30 UVA-LED Flood 370 nm lamps (Loctite, 6.6 –235 $mWcm^{-2}$ irradiance at 15 cm) with controllable irradiance. An EQ CL30 LED Quad Controller (Loctite, ≤ 1500 W) was used to control the irradiance output. The UVA-LED lamp configuration is shown in **Fig. S1a**. The total emitted UVA irradiance across the photoanode used during the experiments was 14.4 or 44.8 $mWcm^{-2}$ and measured using an ocean optics spectrometer (QE65 Pro, 200–1100 nm). **Fig. S1b** shows the UVA irradiance spectrum.

2.6. Photoelectrochemical characterization

The current generated as a function of applied cell potential was measured in the dark and under irradiation. An aqueous solution of Na_2SO_4 (10 mM) was used as a working electrolyte with a conductivity of 2 mS cm^{-1}, like typical secondary treated wastewater conductivity (Rodríguez-Chueca et al., 2015). A DC bench power supply (RS3005 PRO, 0.0–30.0 V ± 20.0 mV) was used to apply voltage ranging from 0.0 to + 1.7 V in + 0.1 V increments. A Duratool digital multimeter

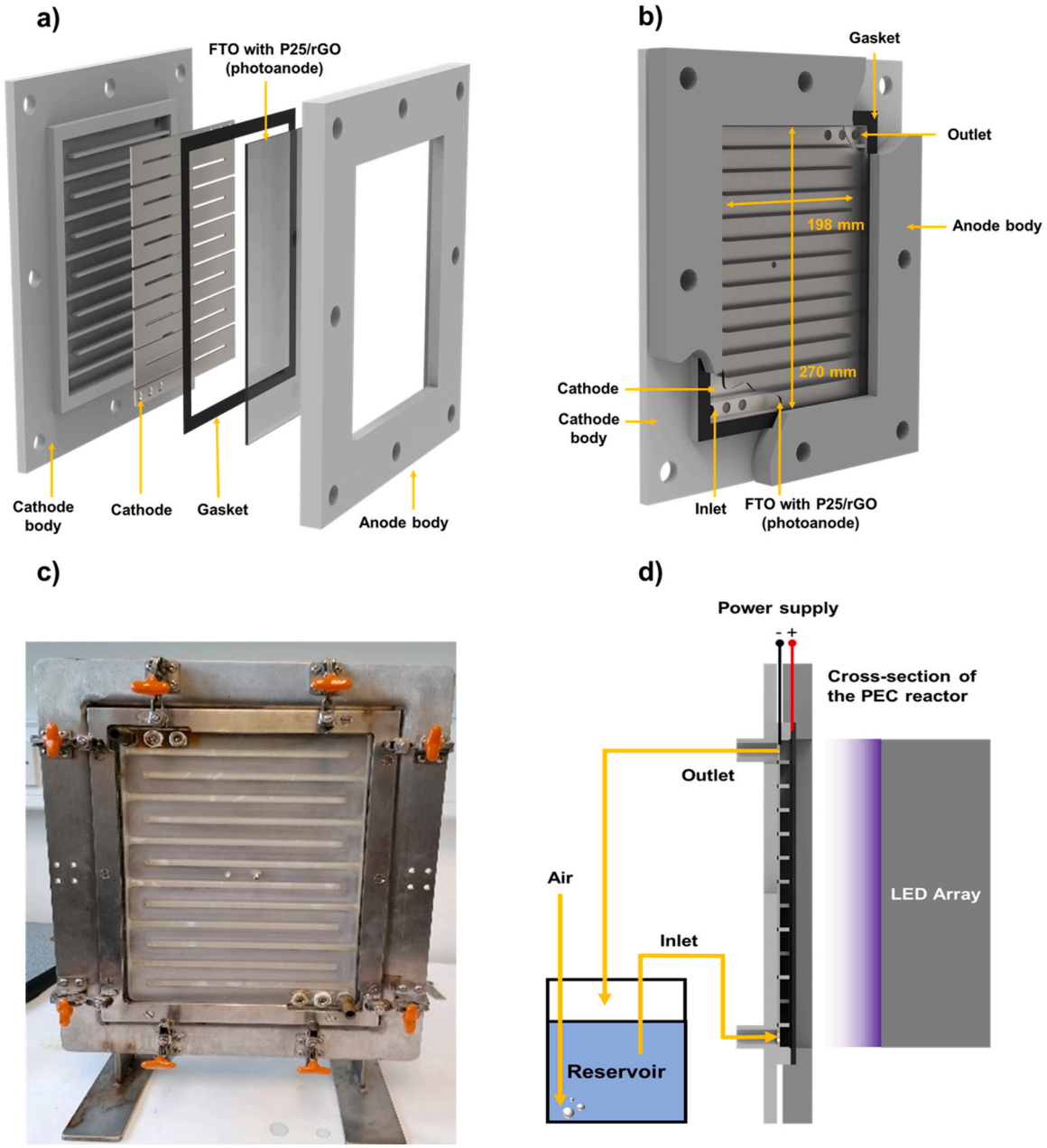

Fig. 1. a) View of the photoelectrochemical reactor, b) assembled view, c) photograph of the reactor, and d) flow diagram of the experimental set-up.

(D03124, 2 $\times 10^{-4}$ –10 A ± 1.5%) was used to monitor the applied potential, and a FLIR DM91 with a data logger multimeter (400 $\times 10^{-4}$ –10 A ± 1%) was used to determine the current.

The current versus time response was recorded during the photoelectrocatalytic degradation of diclofenac at + 1.0 V under both irradiance intensities (14.4 and 44.8 mWcm^{-2}) using an FLIR data logger multimeter. In addition, the current versus time response was recorded during photoelectrocatalytic experiments without the addition of diclofenac under both irradiance intensities for 2 h, to evaluate the stability of the prepared photoanodes.

2.7. Photoelectrocatalytic degradation experiments

All the experiments for photoelectrocatalytic (PEC) diclofenac removal, control tests of electrochemical (EC, dark and applied bias), photocatalytic (PC, light and no applied bias), photolysis (PT, irradiation and without electrodes) and dark (no light neither applied bias and in the presence of the photoanode) performance, were carried out for 2 h in duplicate with an initial concentration of 10 mg/L of diclofenac in 10 mM Na_2SO_4. Dark control experiments were performed for 2 h to evaluate diclofenac pollutant adsorption on the surface of the photoanodes. The diclofenac adsorption over the photoanodes reached a constant value with a 30 min duration (**Fig. S2**). Thus, 30 min was selected as the equilibration time before each degradation experiment in the dark. The reactor set-up is shown in Fig. 1**d** and operated in a recirculating batch mode with a peristaltic pump with a flow rate of 30 mL/s and a reservoir to treat a total volume of 1 L. The reservoir was continuously purged with air using three small aquarium air pumps at 1.25 L/min. The applied potential was based on the maximum photocurrent density obtained from the current at fixed potential characterization which was + 1.0 V. Diclofenac concentration was measured via a UV–Vis spectrophotometer (Spectroquant® Merck Millipore) at 276 nm, by sampling 3 mL from the receiver at 15 min intervals, the sample was returned to the reservoir after measurement to maintain the volume. The stability of the photoelectrodes during degradation was performed via four cycles of PEC using the same photoelectrode with a reaction time of 2 h for each cycle. All the error bars represent the standard error obtained from linear regression analysis of the experimental degradation data fitted to the pseudo-first-order model.

3. Assessment of electrode stability

The current response with time at a fixed cell potential of + 1.0 V was recorded under two irradiance levels (14.4 or 44.8 mWcm^{-2}) for four cycles using a 1% rGO-TiO_2 composite photoanode in 10 mM Na_2SO_4 electrolyte. The duration of each cycle was 1 h. To attempt to electrochemically regenerate the rGO following PEC, the cell was biased negatively at − 1.0 V for 10 min (Toh et al., 2014).

4. Results

4.1. Photocatalytic reduction of GO to form rGO-TiO_2 composites

Changes in GO before and after reduction were visually observed. The color of GO samples changed after photocatalytic reduction from light yellow to grey-black, which indicates a reduction from GO (yellow) to rGO composite (grey-black) (Pei and Cheng, 2011, Mohamed, 2012).

For both 1% and 5% GO samples, a color change was observed (Fig. 2). Pei and Cheng (2011) attributed the color change to the partial restoration of the π bonds within the graphitic carbon structure (Pei and Cheng, 2011), which is a convenient indicator of successful GO reduction and rGO-TiO_2 composite formation by the photocatalytic reduction. A darker color change was observed with the 5% GO, indicating a higher rGO concentration, which was confirmed by Raman spectroscopy in section 3.4.3.

FESEM was used to investigate sample morphology of the P25 TiO_2, 1% rGO-TiO_2, and 5% rGO-TiO_2 electrodes (Fig. 3). The TiO_2 films were formed with micro-aggregates (Fig. 3**a**). As the concentration of GO increased, surface roughness, aggregation, and agglomerate size increased (Fig. 3**c** and **e**) similar observations were reported by others (Pastrana-Martínez et al., 2012; Vallejo et al., 2019). The film thickness was also examined (**Fig. S3**), due to the spray coating method utilised in this work the films are not uniform; subsequently, there appears to be no significant deviation in the thickness between the 3 materials examined all with a loading of 1 mgcm^{-2}.

An increase in agglomeration was observed after the addition of rGO. A similar behaviour was observed in previous studies and was attributed to the removal of oxygen-containing functional groups in rGO, which decreases the electrostatic repulsion between nm particles, inducing aggregation (Chen and Jafvert, 2010; Bitter et al., 2014; Shams et al.,

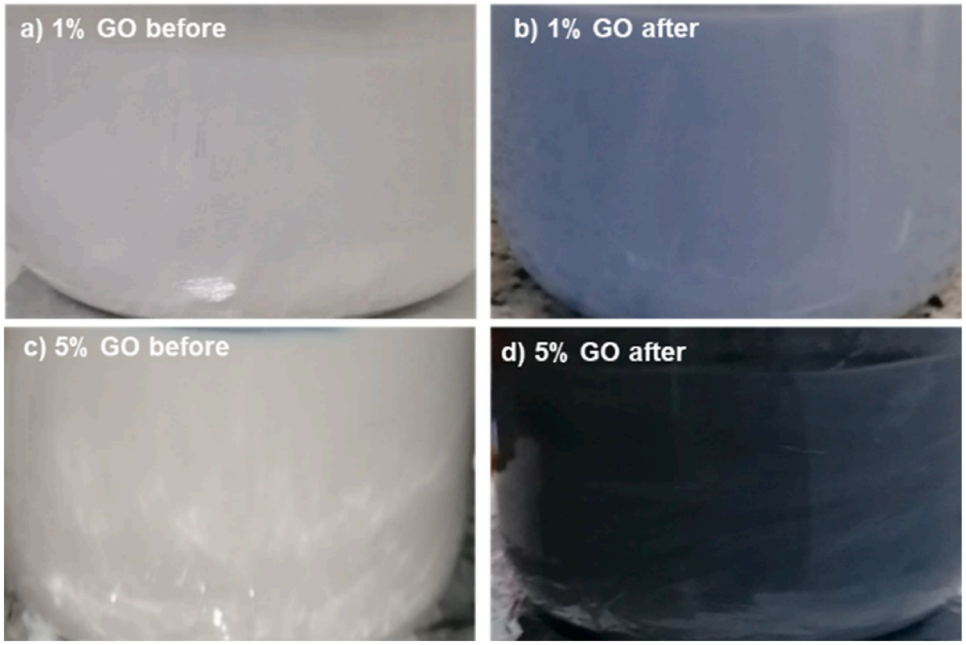

Fig. 2. Colour changes in the GO-TiO_2 suspension before and after 5 h reduction of (a, b) 1% and (c, d) 5% GO.

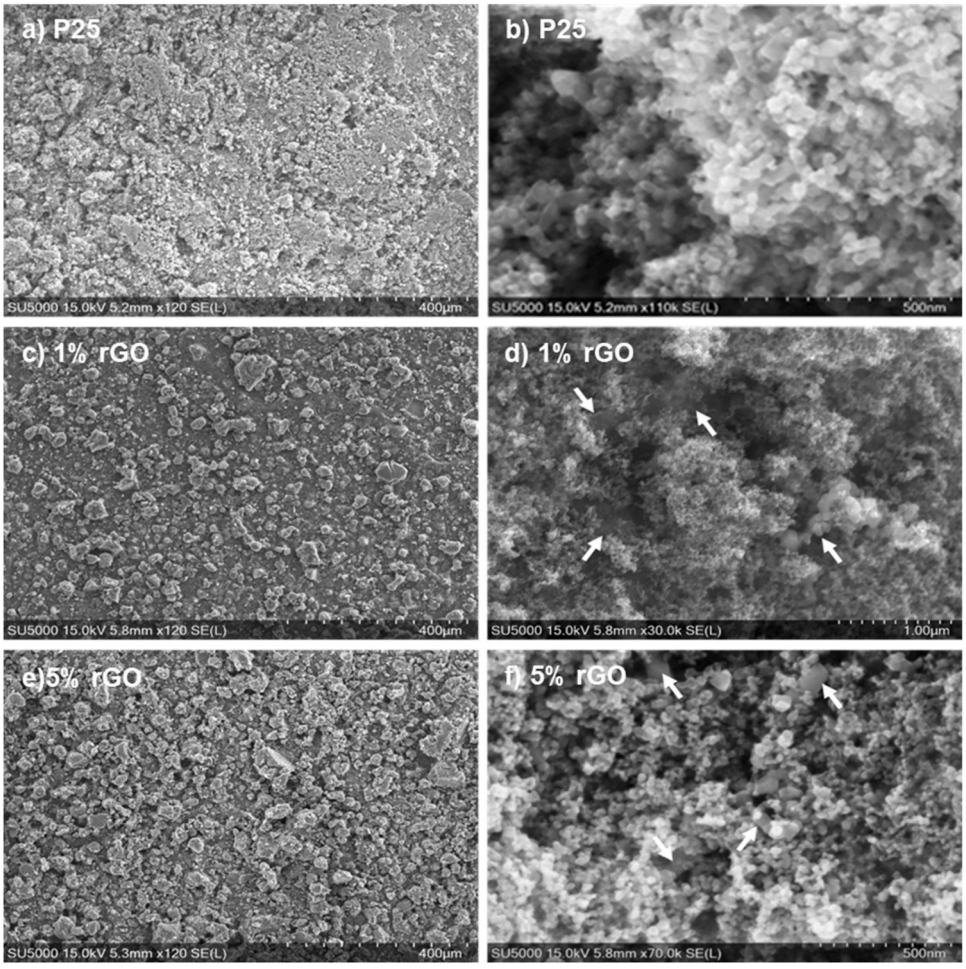

Fig. 3. SEM surface images of (a, b) P25-TiO_2, (c, d) 1% rGO-TiO_2, and (e, f) 5% rGO-TiO_2.

2019). While increased aggregation occurred at higher concentrations of rGO as there was more GO to reduce and subsequently an increased reduction of the oxygen groups at the higher concentration, which was confirmed by Raman spectroscopy in section 3.4.3. The agglomeration process is commonly reported when TiO_2 nanoparticles are combined with graphene sheets (Shams et al., 2019; Vallejo et al., 2019, Tolosana-Moranchel et al., 2019a). In previous studies, it has been found that agglomerates within the rGO-TiO_2 composite can improve photocatalytic activity owing to the enhanced separation of photogenerated charge pairs, which occurs following contact with TiO_2 particles and improves inter-particle charge transfer within the agglomerates (Bitter et al., 2014, Ryu et al., 2015). For example, Ryu et al. (2015) reported that rGO-TiO_2 composite agglomerates promoted acetaldehyde oxidation. Increased FESEM magnification images for P25, 1%, and 5% rGO-TiO_2 electrodes are shown in Fig. 3**b, d,** and **f**. The rGO was observed within the TiO_2 film assembly, which supports previous observations reported for rGO-TiO_2 composite films (D. Wang et al., 2012; P. Wang et al., 2012).

The EDX spectra of TiO_2, GO, 1% rGO-TiO_2, and 5% rGO-TiO_2 composite along with the elemental atomic percentages is shown in **Fig. S4a–d**. The EDX profile for P25 TiO_2 and 5% rGO-TiO_2 composite were also evaluated (**Fig. S4e–f**). Elemental mapping of P25 TiO_2 confirmed the presence of Ti and O as well as a very small amount of C, which indicated sample purity (**Fig. S4a**). For the pure GO sample, C and O were present (**Fig. S2b**). The prepared rGO-TiO_2 composites contained Ti, O, and C elements, which confirmed the presence, purity, and dispersion of rGO in the TiO_2 film, as shown in **Fig. S4c and d**. EDX analysis revealed that the prepared electrodes had no significant impurities and indicated the successful incorporation of rGO with TiO_2 film and increased carbon content at higher rGO/TiO_2 weight ratios (Tolosana-Moranchel et al., 2019b).

4.2. *Photocurrent response of rGO-TiO_2 photoanodes*

The current response at different applied potentials in electrolyte was examined for each photoanode (TiO_2 1% rGO-TiO_2, and 5% rGO-TiO_2), in the dark and then with the light, under 14.4 $mWcm^{-2}$ and 44.8 $mWcm^{-2}$ UVA-LED irradiance in 10 mM Na_2SO_4 electrolyte (Fig. 4). In the dark, the anodic currents were negligible below + 1.1 V, which is a typical response of an n-type semiconductor in contact with an electrolyte (Byrne and Eggins, 1998a), while the observed small increase in current (below 40 μAcm^2) at potentials higher than + 1.1 V in the dark is typically associated with semiconductor breakdown (Tantis et al., 2015). Under UVA-LED irradiation an increased anodic current was observed, i.e., the generation of a photocurrent because of electron photoexcitation to the conduction band. The photocurrent increases upon irradiation and continues to rise with increasing cell potential before levelling off to a saturated photocurrent at + 0.3 V for TiO_2 and + 0.5 V for rGO-TiO_2 composite. The initial rise in photocurrent implies a limitation of electron transport in the semiconductor electrode film. The saturation part indicates several aspects: a limitation of charge carrier diffusion through the semiconductor film (Pablos et al., 2014), the limited photoinduced holes utilization at the electrode surface (Jiang et al., 2007), and the maximum number of photogenerated electrons reaching the ohmic contact of the supporting electrode (Han et al., 2017).

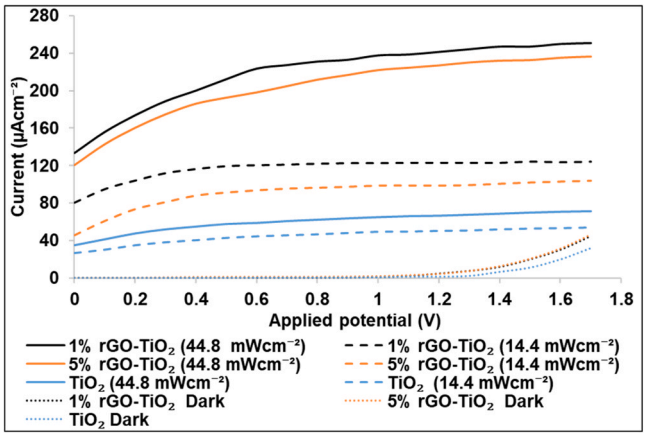

Fig. 4. Currents at different potentials for 1% rGO-TiO_2, 5% rGO-TiO_2, and TiO_2 photoanodes under irradiated (light) and dark conditions. Experimental conditions were as follows: 14.4 & 44.8 $mWcm^{-2}$ irradiance, 10 mM Na_2SO_4 electrolyte, and 0.0 to + 1.7 V cell potential range at + 0.1 V increments.

All rGO-TiO_2 composite electrodes exhibited a higher photocurrent than the unmodified TiO_2 electrode at both irradiances (Fig. 4), implying improved charge carrier separation on the rGO-TiO_2 composite electrodes, improved electron transport through the semiconductor electrode film and higher electronic mobility, as reported by Tayebi et al. (2019), deduced via electrochemical impedance spectroscopy.

The photocurrent density at + 1.0 V cell potential and 14.4 $mWcm^{-2}$ irradiance for TiO_2, 1% rGO-TiO_2, and 5% rGO-TiO_2 composites were 49 ± 1, 122 ± 1.2, and 99 ± 1 μAcm^{-2}, respectively. While the photocurrent density at + 1.0 V cell potential and 44.8 $mWcm^{-2}$ irradiance for TiO_2, 1% rGO-TiO_2, and 5% rGO-TiO_2 composites were 65 ± 1, 237 ± 2.4, and 221 ± 2.2 μAcm^{-2}, respectively. Increasing the intensity resulted in a higher photocurrent for all electrodes due to the higher incident photon flux, which induced higher charge carrier photogeneration (Garcia-Segura et al., 2017). The 1% rGO-TiO_2 composite exhibited the highest photocurrent at both irradiances, while increasing rGO concentration up to 5% reduced the photocurrent. According to P. Wang et al. (2012); D. Wang et al. (2012), increasing the rGO concentration from 1% to 1.5% resulted in a reduction in the current due to the large rGO fraction wrapping TiO_2 leading to higher light absorption by the rGO layer and reduced light intensity reaching the TiO_2 particles i.e., shielding effect, and the increase in recombination sites associated with excessive rGO (D. Wang et al., 2012; P. Wang et al., 2012). The difference in the photocurrent between the 1% and 5% rGO-TiO_2 composites marginally decreased with increasing intensity, yielding a difference of 23 and 15 μAcm^{-2} at 14.4 $mWcm^{-2}$ and 44.8 $mWcm^{-2}$ irradiance levels, respectively, at an applied potential of + 1.0 V due to the lower shielding effect with increasing irradiance.

5. Photoelectrocatalytic degradation of diclofenac

Diclofenac (10 mg/L) was used as a model pollutant. Diclofenac adsorption over the three photoanodes was evaluated as a function of time in the dark and without applying a potential for 2 h. Adsorption equilibration was reached after 30 min (**Fig. S2**) and the total adsorption was 3%, 4.1%, and 4% of the initial concentration of diclofenac for TiO_2, 1% rGO-TiO_2, 5% rGO-TiO_2 composite, respectively. The diclofenac adsorbed was similar for all rGO-TiO_2 composite electrodes, and slightly greater that for the TiO_2 electrode. Diclofenac degradation was also evaluated by photolytic, photocatalytic and PEC under both UV intensities; and electrocatalysis (without irradiation). For photolytic and electrolytic treatment (+1.0 V) diclofenac degradation was negligible within 2 h (**Table S1**). For PC (electrode at open circuit) and PEC, diclofenac degradation was observed within 2 h. The degradation followed a pseudo first order reaction kinetic (see **Fig. S5**). The reaction rate constants (k) and standard errors are presented in **Table S2**. Fig. 5 shows the first-order reaction rate constant (k) for the photocatalytic and photoelectrocatalytic treatment. For the TiO_2 sample, the difference between the rates for PC and PEC was negligible under both irradiance levels (Dale et al., 2009).

Several authors have reported that there is an independent relationship between the applied potential and the photocurrent of P25 photoelectrode due to the presence of nm-sized particles (Byrne and Eggins, 1998a; Pablos et al., 2014), charge trapping sites, and grain boundaries within the P25 TiO_2 material (Jiang et al., 2010). These factors hinder the formation of a depletion layer responsible for the separation of photogenerated charge carriers when a potential is applied. Thus, the obtained photocurrent was attributed to the transport of the charge carrier by diffusion, rather than through the formation of a depletion layer. This leads to a lower impact of the applied potential on the charge carrier separation, which, in turn, results in higher charge recombination, lower ROS generation, and induced photoelectrocatalytic degradation performance.

The results show that the addition of rGO resulted in an improvement in the k for PEC and the difference in the k between the PC and PEC in comparison to TiO_2 at both irradiance levels. The improvement in the TiO_2 degradation and disinfection performance after the addition of rGO has been widely reported in the literature (Wang et al., 2012; Pastrana-Martínez et al., 2012; Cruz-Ortiz et al., 2017). For instance, Wang et al. reported $k = 0.096\ min^{-1}$ for the degradation of Rhodamine dye using rGO-TiO_2 composite under UVA irradiation compared to $0.023\ min^{-1}$ for TiO_2 alone during the PEC process (D. Wang et al., 2012; P. Wang et al., 2012). Cruz-Ortiz et al. (2017) reported 6 log inactivation of E. coli using rGO-TiO_2 suspension in 90 min under UV-Vis irradiance, while the same level of inactivation was achieved by TiO_2 in 120 min. The significant improvement associated with the addition of rGO was attributed to the increased efficiency of charge transport and reduced electron-hole recombination rates (Wang et al., 2012; Pastrana-Martínez et al., 2012; Cruz-Ortiz et al., 2017), which occurred owing to the high electronic conductivity of rGO (D. Wang et al., 2012; P. Wang et al., 2012).

The 1% rGO-TiO_2 composite electrode exhibited a higher degradation performance than 5% rGO-TiO_2 for PC at both irradiance levels, while an insignificant difference between rGO loadings was observed with PEC. Numerous studies have attributed the reduced performance of high rGO loading to the large rGO fraction wrapping TiO_2 leading to higher light absorption by the rGO layer and reduced light intensity reaching the TiO_2 particles i.e., shielding effect (Villajos et al., 2021, González et al., 2022), and the function of excessive rGO as recombination centre (Wang et al., 2012; Minella et al., 2017). Thus, the photocatalytic performance diminished with the higher rGO loading. As reported in the literature, the application of potential can improve charge carrier separation and enhance ROS generation (Daghrir et al., 2012), which can lead to improved degradation performance for the high rGO concentrations during the PEC, resulting in a similar performance for both rGO concentrations. In addition, increasing the intensity resulted in a significant increase in the photocurrent, but there was only a marginal improvement in the rate of diclofenac degradation. Li et al. (2013) observed a decrease in photoelectrocatalytic uridine degradation by TiO_2 photoanode with increasing the intensity beyond 20 $mWcm^{-2}$. This decrease was attributed to the higher current efficiency towards water oxidation rather than ROS generation (Li et al., 2013; Nakabayashi and Nosaka, 2013).

The proposed primary reactions occurring at the rGO-TiO_2 photoanode, when illuminated and biased with a potential greater than the bandgap, are shown in reactions 1–10. The application of a potential exceeding the flat band potential of the semiconductor photocatalyst facilitates efficient electron (e^-) and hole (h^+) separation (reaction 1), minimizing recombination rates (reaction 2). This process promotes the migration of h^+ toward the photoanode surface. Upon reaching the

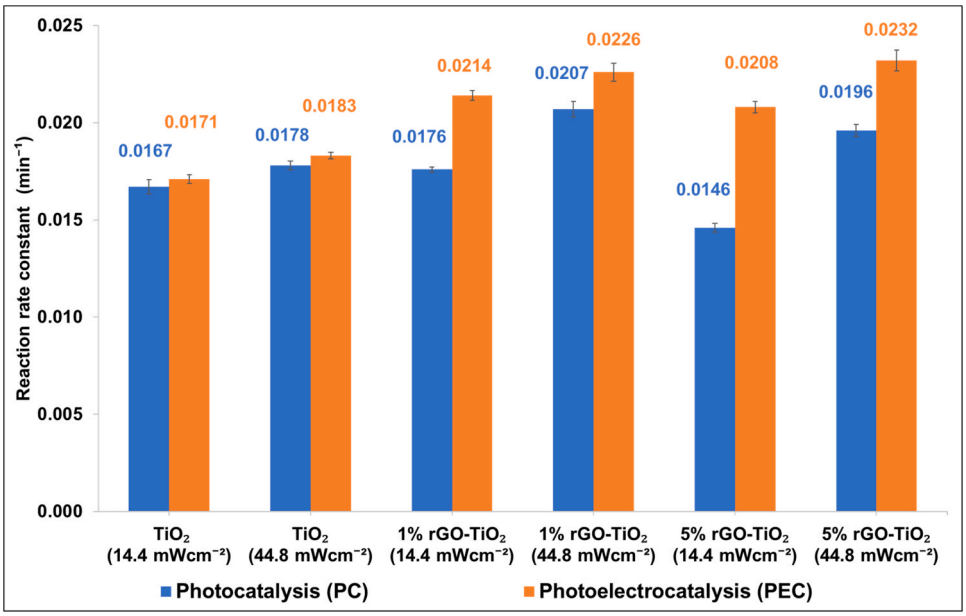

Fig. 5. First-order reaction rate constants for diclofenac degradation for PC and PEC processes using TiO_2, 1% rGO-TiO_2, and 5% rGO-TiO_2 composite photoanodes. Experimental conditions: 14.4 and 44.8 $mWcm^{-2}$ irradiances, 10 mM Na_2SO_4 electrolyte, 2 h reaction time, + 1.0 V applied potential for PEC, and 10 mg/L diclofenac.

photocatalyst surface, h+ either directly oxidize diclofenac (reaction 3 and 4) or initiate the generation of $HO^{\bullet}$ through HO^- and water oxidation (reactions 5 and 6). Furthermore, these h^+ may oxidize water to produce oxygen (reaction 7). Conversely, e^- in the conduction band engage in reduction reactions, generating ROS through various oxygen reduction reactions such as $O_2^{\bullet-}$ (reaction 8), hydroperoxyl radicals ($HO_2^{\bullet}$) (reaction 9), or hydrogen peroxide (H_2O_2) (reaction 10). Additionally, $HO^{\bullet}$ can be formed from H_2O_2 (reactions 11 and 12). the generated ROS promote the efficient degradation Diclofenac by PEC, resulting in the production of H_2O and CO_2 (reactions 13) (McMichael et al., 2021, Joseph and Vijayanandan 2023, Cruz-Ortiz et al., 2017, Sanchez Tobon et al., 2022)

$$rGO - TiO_2 + h\nu \rightarrow e^-_{BC} + h^+_{VB} \quad (1)$$

$$e^-_{BC} + h^+_{VB} \rightarrow Energy(heat) \quad (2)$$

$$h^+_{BV} + Diclofenac \rightarrow Diclofenac^{\bullet+} \quad (3)$$

$$Diclofenac^{\bullet+} \rightarrow H_2O + CO_2 \quad (4)$$

$$h^+_{VB} + H_2O \rightarrow HO^{\bullet} + H^+ \quad (5)$$

$$h^+_{VB} + HO^- \rightarrow HO^{\bullet} \quad (6)$$

$$2H_2O + 4h^+_{BV} \rightarrow O_2 + 4H^+ \quad (7)$$

$$e^-_{BC} + O_2 \rightarrow O_2^{\bullet-} \quad (8)$$

$$O_2^{\bullet-} + H^+ \rightarrow HO_2^{\bullet} \quad (9)$$

$$2HO_2^{\bullet} \rightarrow H_2O_2 + O_2 \quad (10)$$

$$H_2O_2 + O_2^{\bullet-} \rightarrow HO^{\bullet} + O_2 + HO^- \quad (11)$$

$$H_2O_2 + e^-_{Cb} \rightarrow HO^{\bullet} + HO^- \quad (12)$$

$$Diclofenac + ROS \rightarrow H_2O + CO_2 \quad (13)$$

Also, the energy consumption for the photocatalytic and photoelectrocatalytic treatment was evaluated (**Table S3**). PEC exhibited a lower energy consumption than the PC due to the improvement in the degradation performance of diclofenac. However, as the intensity increased, both PEC and PC required higher energy input to degrade diclofenac. Among the different photoelectrodes, the 1% rGO-TiO_2 photoanode PEC showed the lowest energy consumption at 14.4 mW cm^{-2} irradiance (0.417 kWh L^{-1} $order^{-1}$). Thus the 1% rGO-TiO_2 composite was selected as the best photoanode candidate to work with an irradiation intensity of 14.4 $mWcm^{-2}$ for best energy efficiency.

A comparative analysis of the degradation performance of diclofenac using the rGO-TiO_2 photoanode in the present study and a previously reported photoanode based on rGO-TiO_2 in a PEC process is presented in (**Table S4**). Although direct comparison is challenging due to variations in experimental conditions, the photoanode employed in this study demonstrated exceptional performance when compared to other rGO-TiO_2 based photoanode reported in literature. Notably, the rGO-TiO_2 exhibited remarkable performance in this work, highlighting its efficacy in PEC application.

5.1. rGO-TiO_2 electrode stability

For any proposed solution for water treatment, it is important to assess the stability of the materials used. Therefore, to evaluate the stability of rGO photoanodes, several investigations were conducted, which include changes in the photocurrent after degradation; differences in kinetic values when the photoanode is reused; and characterization of the rGO using XPS and Raman spectroscopy.

5.1.1. Photocurrent stability

The photocurrent response was assessed before and after PC and PEC experiments (Fig. 6**a** & **Fig. S6**). A decrease in photocurrent was observed after the PEC and PC experiments using rGO-TiO_2 electrodes. At an irradiance of 14.4 $mWcm^{-2}$ and an applied bias of + 1.0 V, both 1% and 5% rGO-TiO_2 electrodes exhibited a decrease in photocurrent of 17.4 μAcm^{-2} (14%) and 15.9 μAcm^{-2} (16%), respectively. Similarly, at an irradiance of 44.8 $mWcm^{-2}$ and an applied bias of + 1.0 V, the photocurrent for both 1% and 5% rGO-TiO_2 electrodes decreased by 36 μAcm^{-2} (16%) and 40 μAcm^{-2} (18%), respectively.

The photo-oxidation and degradation of rGO have been demonstrated by several authors (Akhavan et al., 2010; Radich and Kamat, 2013; Spilarewicz-Stanek et al., 2021; Mondal et al., 2021), who

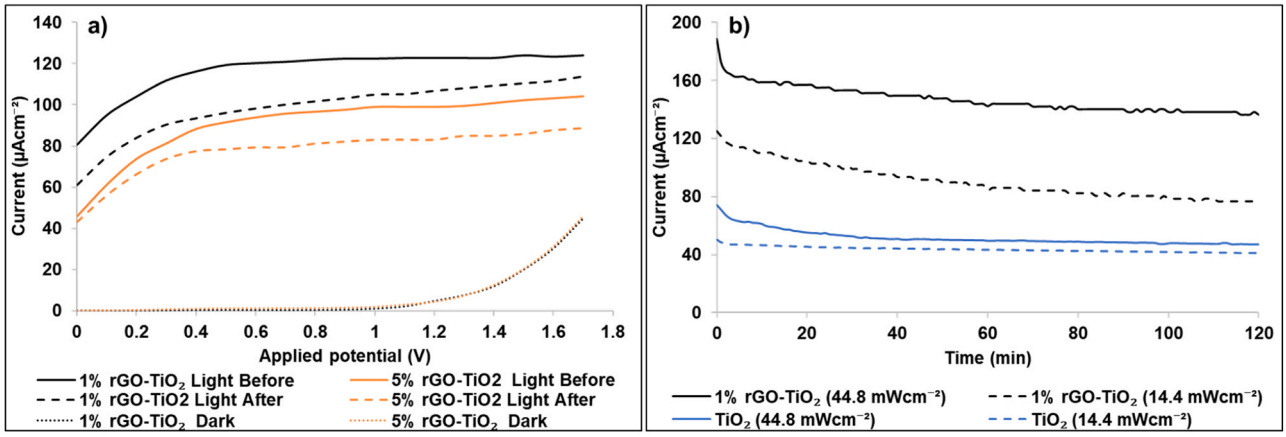

Fig. 6. a) Current at various fixed potentials for 1% and 5% rGO-TiO_2 anodes before and after diclofenac photocatalytic degradation experiments under irradiation with 14.4mWcm^{-2} (light) and dark conditions b) Photocurrent–time response of TiO_2, 1% rGO-TiO_2 composites under 14.4 & 44.8 mWcm^{-2}. Experimental conditions were as follows: 10 mM Na_2SO_4 electrolyte a) 0.0 V to + 1.7 V cell potential range at + 0.1 V increments b), 2 h experiment duration, + 1.0 V applied potential.

reported the rGO photo-oxidation and degradation in the rGO-TiO_2 composite by $OH^{\bullet}$ generated by the photoexcited TiO_2, during irradiation of an electrode immersed in water yielding the defragmentation of rGO and emission of CO_2. Furthermore, the higher drop in the photocurrent observed with increasing intensity may be attributed to faster rGO degradation and photo-oxidation. Spilarewicz-Stanek et al. (2021) reported that the coverage of TiO_2 surface by GO decreased with increasing UV dose, which was attributed to the faster degradation of the GO (Spilarewicz-Stanek et al., 2021). In addition, a higher relative decrease in the photocurrent was observed with the 5% rGO-TiO_2 composite as compared to the 1% composite at both irradiances which can be due to the higher photo-oxidation and degradation associated with high rGO concentration.

The photocurrent-time response in absence of diclofenac was investigated for TiO_2 and 1% rGO-TiO_2 composite under both intensities (14.4, and 44.8 mWcm^{-2}) (Fig. 6**b**). For the 1% rGO-TiO_2 composite at both irradiance levels, the photocurrent-time response was recorded for a period of 2 h, a continuous decay in the photocurrent over time without reaching a steady-state photocurrent confirming the degradation (Selvaraj et al., 2016) and photo-oxidation of rGO.

During the PEC degradation of diclofenac the current was recorded (**Fig.S6b**). The photocurrent was higher in the presence of diclofenac and electrolyte (**Fig.S6b**) compared to that in presence of the electrolyte alone (Fig. 6**b**). For all electrodes, under both irradiance levels, the photocurrent decay over time occurred due to the degradation of diclofenac. However, in the case of the rGO-TiO_2 composite, the decay in the photocurrent–time response was also due to the degradation of rGO over time, though the degradation of rGO occurred more slowly in the presence of diclofenac due to the competition between the rGO and pollutant towards $HO^{\bullet}$.

6. Electrode stability over repeat cycles of photoelectrocatalytic treatment

The reusability & stability of the 1% and 5% rGO-TiO_2 photoanodes were investigated over four cycles of diclofenac degradation, with a duration of 2 h per cycle under 14.4 mWcm^{-2} irradiance (Fig. 7). The reaction rate constant (k) for diclofenac degradation for both rGO-TiO_2 composite electrodes revealed a notable decrease with each PEC experiment. The k value dropped after the fourth cycle, from 0.0220 to 0.0208 min^{-1} for the 1% rGO-TiO_2 and from 0.0224 to 0.0194 min^{-1} for the 5% rGO-TiO_2.

Several articles have been published based on rGO-TiO_2 composites as photocatalysts in PC and PEC. However, many of these papers do not report the stability of the composite (Tolosana-Moranchel et al., 2019a and 2019b; Mohammadi et al., 2019; Carreño-Lizcano et al., 2020). Studies that do report on stability indicate that the material is stable, although a clear decrease in degradation performance has been observed over time (Wang et al., 2012; Zuo et al., 2021). Further analysis using XPS and Raman was performed to better understand molecular changes in the rGO-TiO_2 composite after PEC treatment.

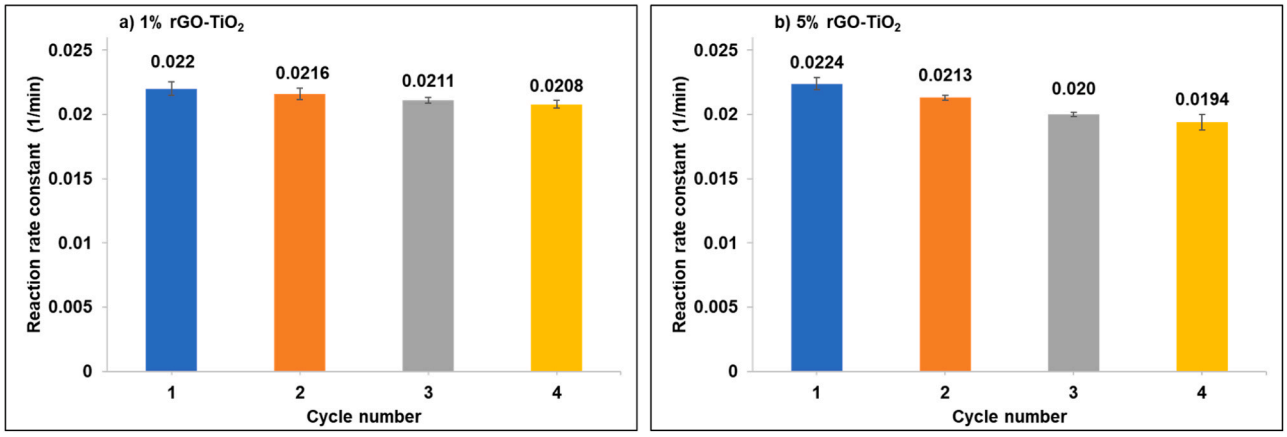

Fig. 7. PEC stabilities using a) 1% rGO-TiO_2 and b) 5% rGO-TiO_2 for four cycles. Experimental conditions were as follows: 14.4 mWcm^{-2} irradiance, 10 mM Na_2SO_4 electrolyte, 2 h reaction time, + 1.0 V applied potential, and 10 mg/L diclofenac.

6.1. XPS & Raman characterization before and after experiments

Fig. 8 shows the Raman spectra of GO, 1% rGO-TiO_2, and 5% rGO-TiO_2 composite before and after diclofenac photocatalytic degradation experiments. The main characteristic bands of carbonaceous material in Raman spectra are the D band at 1360 cm^{-1} ascribed to sp^3 hybridization and disorder or defects in the sp^2-hybridized carbon atoms, the G band at 1600 cm^{-1} attributed to the vibration of ordered sp^2 carbon atoms (Monteagudo et al., 2019, Spilarewicz-Stanek et al., 2021), 2D band at 2670 cm^{-1} attributed to second-order dispersive Raman mode and the presence of a multi-graphene layer; and the combination of D+G as stated before at 2940 cm^{-1} (Xu and Cheng, 2013, Monteagudo et al., 2019). The intensity ratio of I_D and I_G peaks were analyzed, revealing defects in the carbon structures and the reduction degree. As the I_D/I_G ratio increased, defects increased i.e. a higher degree of GO reduction and successful oxygen functional group removal.

Table 1 shows the prepared electrode I_D/I_G ratio before and after diclofenac PEC and PC degradation experiments. The I_D/I_G of the GO, 1% rGO-TiO_2, and 5% rGO-TiO_2 composite before degradation experiments increased from 0.89 to 1.32 and 1.37, respectively, which confirms the increase in the incidence of defects on the GO surface due to the removal of oxygen functional groups and successful reduction to rGO. Moreover, the reduction degree was slightly higher for the 5% rGO-TiO_2 composite due to the strong interactions between TiO_2 and GO sheets at higher concentrations (Mohammadi et al., 2019). However, the I_D/I_G decreased after the PEC and PC degradation experiments to 1.03 and 1.06 for 1% and 5% rGO-TiO_2 respectively, which indicates reoxidation of the rGO and oxygen functional group restoration (Spilarewicz-Stanek et al., 2021; Mondal et al., 2021). In addition, a decrease in the intensity of Raman spectra bands for rGO-TiO_2 composite electrodes following diclofenac PEC and PC degradation experiments as shown in Fig. 8 can be attributed to rGO oxidation (Akhavan et al., 2010; Spilarewicz-Stanek et al., 2021).

XPS analysis was performed to evaluate the elemental composition and chemical state of rGO-TiO_2 composite electrodes. Table 2 shows the elemental atomic percentage results obtained from the XPS analysis for the rGO-TiO_2 composite electrodes before and after diclofenac photocatalytic degradation experiments. After the experiments, the carbon content decreased for rGO-TiO_2 composites, while the oxygen content increased. The decrease in carbon content was more significant at higher GO loadings due to the increased interaction with TiO_2, which promoted degradation. The 5% rGO-TiO_2 composite exhibited a higher C/O ratio compared to the 1% rGO-TiO_2 composite due to the higher rGO/TiO_2 ratio (Mohammadi et al., 2019). These results correlate with the Raman spectroscopy results indicating rGO reoxidation.

To confirm variation in the oxygen functional group composition of the GO and rGO-TiO_2 composites, XPS C 1 s spectra were acquired. **Fig. S8** depicts the XPS spectra of C1s for GO and rGO-TiO_2 composites before and after diclofenac PEC and PC degradation experiments. The deconvolution of peaks centred at binding energy levels 288.4, 284.7, 286.3, and 288.5 eV were attributed to C-C/C═C in aromatic rings, C-O (epoxy and hydroxyl groups), and C═O (carbonyl and carboxylic groups), respectively (Tayebi et al., 2019).

The atomic percentages of chemical states for C1s XPS spectra are shown in Table 3. Before diclofenac PEC and PC degradation experiments, the (C–C, C═C)/C–O and (C–C, C═C)/C═O ratios increased for both rGO-TiO_2 electrodes compared to GO due to the removal of the oxygen-containing groups and an increase in the C–C/C═C content with respect to other functional groups, thus confirming the successful reduction of GO to rGO. However, these ratios decreased after the photocatalytic and photoelectrocatalytic experiments due to the reoxidation of the rGO (Peng et al., 2016). Before diclofenac PEC and PC degradation experiments, the 5% rGO-TiO_2 had a higher C–C/C═C atomic percentage and higher percentage removal of oxygen functional groups compared to the 1% rGO-TiO_2 composite, indicating a slightly higher reduction degree at increasing concentrations due to increased interaction between TiO_2 and GO (Mohammadi et al., 2019). Furthermore, C═O removal was lower than that of C-O for both rGO-TiO_2 composites due to the higher stability of carbonyl and carboxylic groups (C═O), which are less likely to react initially and higher C-O contents, which are more exposed for reduction (Shams et al., 2019; Taniguchi et al., 2021; Spilarewicz-Stanek et al., 2021). The C═O remained almost stable for the 1% rGO-TiO_2 composite, while for the 5% rGO, C═O slightly decreased due to the stronger interaction between GO and TiO_2 at a higher concentration, which leads to increased reduction and

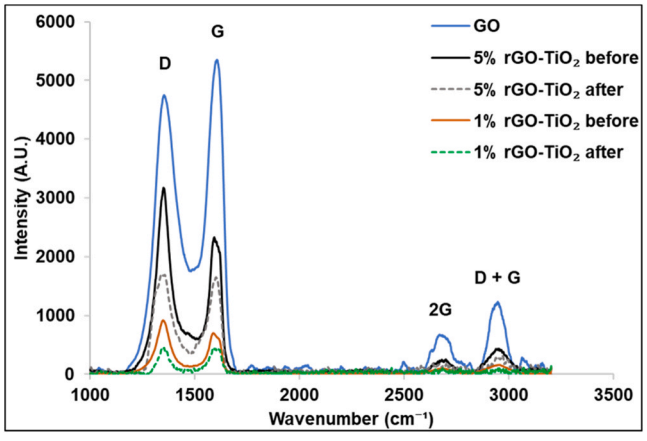

Fig. 8. Raman spectra of GO, 1% rGO-TiO_2, and 5% rGO-TiO_2 before and after diclofenac photocatalytic degradation experiments.

Table 1
Comparison of Raman spectra peak ratios (I_D/I_G) for GO, 1% rGO-TiO_2, and 5% rGO-TiO_2 composite before and after diclofenac photocatalytic degradation experiments.

	GO	1% rGO-TiO_2	5% rGO-TiO_2
Before PEC	0.89	1.32	1.37
After PEC	-	1.03	1.06

Table 2
XPS elemental analyses of the 1% and 5% rGO-TiO_2 before and after diclofenac photocatalytic degradation experiments.

	C1s (%)	O1s (%)	Ti2p (%)	C/O
1% rGO-TiO_2 before PEC	4.0 ± 0.5	65.3 ± 0.3	30.7 ± 0.6	0.06
1% rGO-TiO_2 after PEC	2.7 ± 0.7	67.3 ± 0.8	30.1 ± 0.5	0.04
5% rGO-TiO_2 before PEC	16.3 ± 1.0	57.9 ± 1.3	25.8 ± 0.7	0.28
5% rGO-TiO_2 after PEC	10.5 ± 1.7	62.3 ± 1.7	27.2 ± 0.9	0.17

Table 3
Atomic percentages of chemical states for C 1 s spectra before and after diclofenac photocatalytic degradation experiments (data shown are averages of three measurements).

	C–C, C═C (%) (284.4 eV)	C–O (%) (286.3 eV)	C═O (%) (288.5 eV)	(C-C, C═C) / C–O	(C-C, C═C) / C═O
GO	39.4 ± 2.8	40.7 ± 1.5	19.9 ± 1.5	1.0	2.0
1% rGO-TiO_2 before	72.5 ± 1.3	6.4 ± 3.0	21.1 ± 1.7	11.3	3.4
1% rGO-TiO_2 after	61.5 ± 2.1	17.1 ± 2.7	21.4 ± 3.0	3.6	2.9
5% rGO-TiO_2 before	78.2 ± 3.1	7.8 ± 1.6	14.0 ± 1.5	10.0	5.6
5% rGO-TiO_2 after	64.8 ± 1.1	22.0 ± 1.0	13.2 ± 1.4	2.9	4.9

oxygen functional group removal (Shams et al., 2019; Mohammadi et al., 2019). After the experiments, the C-O functional groups partially recovered due to reoxidation, and the C═O groups remained nearly stable. The proposed routes for rGO degradation and reoxidation have been reported by other authors. It involves $HO^{\bullet}$ attacks the unsaturated bonds of C═C by an electrophilic addition reaction, introducing large quantities of hydroxyl groups C-OH, i.e. rGO is hydroxylated by $HO^{\bullet}$. In the second step, hydroxyl groups C-OH are further oxidized to C═O, which is then further oxidized and converted into CO_2 and H_2O (Li et al., 2005; Zhou et al., 2012). Thus, these results indicate the reoxidation, degradation, and low stability of rGO-TiO_2 composite in PEC and PC processes.

7. Attempt to electrochemical regenerate the rGO in-situ

As the rGO is being re-oxidized during the PC and PEC experiments, electrochemical reduction of the 1% rGO-TiO_2 electrode after the PEC degradation experiment was examined as a method to regenerate the rGO in-situ. The stability was evaluated by measuring the photocurrent response over four cycles under 14.4 and 44.8 mW cm^{-2} irradiance in 10 mM Na_2SO_4 only. After the first three cycles, the electrochemical reduction was attempted by biasing the cell negative at − 1.0 V for 10 min (Toh et al., 2014). Fig. 9 shows the photocurrent response with time for the four cycles under both irradiance levels. A clear decrease in the photocurrent was observed with time and after each cycle for both irradiance levels, confirming the decomposition of rGO by the generated ROS. However, this decrease was higher at 44.8 $mWcm^{-2}$ due to increased ROS generation.

The decrease in the current at various fixed potentials before and after the electrochemical reduction experiments under the two irradiance levels was evaluated, as shown in **Fig. S9**. The current at an applied potential of + 1.0 V dropped from 117.8 ± 1.2–108.8 μAcm^{-2} ± 1.1 (−7.6%) and 230.5 ± 2–183.8 ± 2 μAcm^{-2} (−20.2%) for 14.4 and 44.8 $mWcm^{-2}$ irradiance levels, respectively. Unfortunately, the electrochemical reduction did not re-establish the original photocurrent response and it can be assumed that the in-situ electrochemical reduction did not regenerate the rGO. Of course, it is likely that the original site of photocatalytic reduction in the formation of the rGO-TiO_2 composites takes place at a reduction site on the TiO_2 surface. This results in a surface bond between the Ti and carbon in the rGO and blocks the reduction site on the surface of the TiO_2. In subsequent use for PC or PEC, the rGO may be oxidized by hydroxyl radicals at a different site near oxidation sites on the TiO_2 surface.

8. Conclusions

rGO-TiO_2 composites were formed by the photocatalytic reduction of GO. The rGO-TiO_2 composites were immobilised on FTO to be used as photoanodes in a bench-scale photoelectrocatalytic reactor for the degradation of diclofenac as a model CEC. The surface modification of TiO_2 with rGO improved the photocurrent response and led to a improved rate of photocatalytic and photoelectrolytic degradation of diclofenac. Additionally, PEC using 1%, and 5% rGO electrodes exhibited 13%, and 16% lower energy efficiency for the process than PC under 14.4 and 44.8 $mWcm^{-2}$, respectively. The best-performing photoanode was 1.0% rGO to TiO_2 under 14.4 $mWcm^{-2}$ irradiance, exhibiting a photocurrent of 122 μAcm^{-2}, and a PEC first-order reaction rate constant (k) of 0.0214 min^{-1} , and energy order of 0.417 kWh L^{-1} $order^{-1}$. However, increasing the rGO concentration to 5% did not further improve the reaction rate constant due to the shielding effect and increased recombination centre associated with high rGO concentration.

The photocurrent decreased over time and over cycles indicating non-stability of the rGO-TiO_2 electrodes. Re-oxidation of the rGO following photocatalytic or photoelectrocatalytic treatment was confirmed by Raman spectroscopy and XPS. Attempts to regenerate the rGO in-situ by electrochemical reduction were not successful, probably due to oxidation of the rGO being at different sites on than those targeted in the photocatalytic reduction of GO in the preparation of the composites. This work indicates the potential to use composite materials to improve the photoelectrocatalytic properties of TiO_2 electrodes but highlights the challenges of stability. The work also demonstrates the ability to scale up photoelectrocatalytic reactors for water treatment and to drive these using UVA LED arrays as a more environmentally friendly approach to Hg lamps.

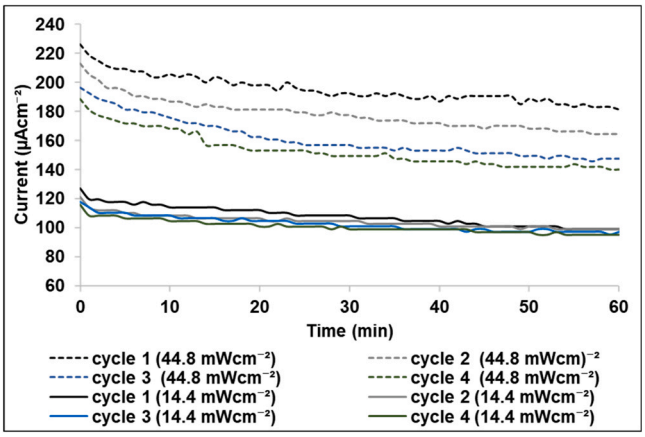

Fig. 9. Photocurrent time responses after four cycles (1 h each) of electrochemical regeneration of 1% rGO-TiO_2 at 14.4 and 44.8 $mWcm^{-2}$, 10 mM Na_2SO_4, + 1.0 V.

CRediT authorship contribution statement

S. Alkharabsheh: Conceptualisation, Methodology, Investigation, Writing - Original Draft, Writing - review & editing. **S. McMichael**: Methodology and Writing - review & editing. **A. Singhal**: Methodology. **A.Rioja-Cabanillas:** Writing - review & editing. **P. Zamora**: Writing - review & editing. **V. Monsalvo**: Funding acquisition, Supervision, Writing - review & editing. **P. Fernandez-Ibanez**: Funding acquisition, Supervision, Writing - review & editing. **J.A. Byrne**: Funding acquisition, Supervision, Writing - review & editing.

Declaration of Competing Interest

The authors declare that they have no known competing financial interests or personal relationships that could have appeared to influence the work reported in this paper.

Acknowledgements

We wish to thank the Marie Curie European H2020 Research and Innovation Action (H2020-MSCA-ITN-EID-812574) for funding this research under the REWATERGY. We thank Pro-Photonix Ltd. (Ireland) for the UVA-LED source design, setting up, and technical support.

Appendix A. Supporting information

Supplementary data associated with this article can be found in the online version at doi:10.1016/j.psep.2023.12.009.

References

Akhavan, O., Abdolahad, M., Esfandiar, A., Mohatashamifar, M., 2010. Photodegradation of graphene oxide sheets by TiO_2 nanoparticles after a photocatalytic reduction. J. Phys. Chem. C. 114 (30), 12955–12959. https://doi.org/10.1021/jp103472c.

Alulema-Pullupaxi, P., Espinoza-Montero, P.J., Sigcha-Pallo, C., Vargas, R., Fernández, L., Peralta-Hernández, J.M., Paz, J.L., 2021. Fundamentals and applications of photoelectrocatalysis as an efficient process to remove pollutants

from water: a review. Chemosphere 281, 130821. https://doi.org/10.1016/j.chemosphere.2021.130821.
Bitter, J.L., Yang, J., Beigzadeh, M.S., Jafvert, C.T., Fairbrother, D.H., 2014. Transformations of oxidized multiwalled carbon nanotubes exposed to UVC (254 nm) irradiation. Environ. Sci. Nano. 1 (4), 324–337. https://doi.org/10.1039/C4EN00073K.
Byrne, J.A., Eggins, B.R., 1998a. Photoelectrochemistry of oxalate on particulate TiO_2 electrodes. J. Electroanal. Chem. 457 (1–2), 61–72. https://doi.org/10.1016/S0022-0728(98)00304-0.
Byrne, J.A., Eggins, B.R., Brown, N.M.D., McKinney, B., Rouse, M., 1998b. Immobilisation of TiO_2 powder for the treatment of polluted water. Appl. Catal. B Environ. 17 (1–2), 25–36. https://doi.org/10.1016/S0926-3373(97)00101-X.
Carreño-Lizcano, M.I., Gualdrón-Reyes, A.F., Rodríguez-González, V., Pedraza-Avella, J. A., Niño-Gómez, M.E., 2020. Photoelectrocatalytic phenol oxidation employing nitrogen doped TiO_2-rGO films as photoanodes. Catal. Today 341, 96–103. https://doi.org/10.1016/j.cattod.2019.02.006.
Chen, C.Y., Jafvert, C.T., 2010. Photoreactivity of carboxylated single-walled carbon nanotubes in sunlight: reactive oxygen species production in water. Environ. Sci. Technol. 44 (17), 6674–6679. https://doi.org/10.1021/es101073p.
Cruz-Ortiz, B.R., Hamilton, J.W.J., Pablos, Díaz-Jiménez, L., Cortés-Hernández, D.A., Sharma, P.K., Castro-Alférez, M., Fernández-Ibañez, P., Dunlop, P.S.M., Byrne, J.A., 2017. Mechanism of photocatalytic disinfection using titania-graphene composites under UV and visible irradiation. Chem. Eng. J. 316, 179–186. https://doi.org/10.1016/j.cej.2017.01.094.
Daghrir, R., Drogui, P., Robert, D., 2012. Photoelectrocatalytic technologies for environmental applications. J. Photochem. Photobiol. A Chem. 238, 41–52. https://doi.org/10.1016/j.jphotochem.2012.04.009.
Dale, G., Hamilton, J., Dunlop, P., Byrne, J.A., 2009. Electrochemically assisted photocatalysis on anodic titania nanotubes. Curr. Top. Electrochem 14, 89–97.
Dunlop, P.S.M., Galdi, A., McMurray, T.A., Hamilton, J.W.J., Rizzo, L., Byrne, J.A., 2010. Comparison of photocatalytic activities of commercial titanium dioxide powders immobilised on glass substrates. J. Adv. Oxid. Technol. 13 (1), 99–106. https://doi.org/10.1515/jaots-2010-0113.
Fernandez-Ibanez, P., McMichael, S., Rioja Cabanillas, A., Alkharabsheh, S., Tolosana-Moranchel, A., Byrne, J.A., 2021. New trends on photoelectrocatalysis (PEC): nanomaterials, wastewater treatment and hydrogen generation. Curr. Opin. Chem. Eng. 34, 100725 https://doi.org/10.1016/j.coche.2021.100725.
Fernández-Ibáñez, P., Polo-López, M.I., Malato, S., Wadhwa, S., Hamilton, J.W.J., Dunlop, P.S.M., D'Sa, R., Magee, E., O'Shea, K., Dionysiou, D.D., Byrne, J.A., 2015. Show moreSolar photocatalytic disinfection of water using titanium dioxide graphene composites. Chem. Eng. J. 261, 36–44. https://doi.org/10.1016/j.cej.2014.06.089.
Garcia-Segura, S., Tugaoen, H.O., Hristovski, K., Westerhoff, P., 2017. Photon flux influence on photoelectrochemical water treatment. Electrochem. Commun. 87, 63–65. https://doi.org/10.1016/j.elecom.2017.12.026.
González, V.J., Vázquez, E., Villajos, B., Tolosana-Moranchel, A., Duran-Valle, C., Faraldos, M., Bahamonde, A., 2022. Eco-friendly mechanochemical synthesis of titania-graphene nanocomposites for pesticide photodegradation. Sep. Purif. Technol. 289, 120638 https://doi.org/10.1016/j.seppur.2022.120638.
Han, Y., Zhang, L., Wang, Y., Zhang, H., Zhang, S., 2017. Photoelectrocatalytic activity of an ordered and vertically aligned TiO_2 nanorod array/BDD heterojunction electrode. Sci. Bull. 62 (9), 619–625. https://doi.org/10.1016/j.scib.2017.03.009.
Jiang, D., Zhang, S., Zhao, H., 2007. Photocatalytic degradation characteristics of different organic compounds at TiO_2 nanoporous film electrodes with mixed anatase/rutile phases. Environ. Sci. Technol. 41 (1), 303–308. https://doi.org/10.1021/es061509i.
Jiang, G., Lin, Z., Zhu, L., Ding, Y., Tang, H., 2010. Preparation and photoelectrocatalytic properties of titania/carbon nanotube composite films. Carbon 48 (12), 3369–3375. https://doi.org/10.1016/j.carbon.2010.05.029.
Joseph, A., Vijayanandan, A., 2023. Plant-based synthesis of TiO2–rGO nanocomposite for the efficient photocatalytic degradation of an emerging contaminant: Experimental and theoretical investigations. Sustain. Mater. Technol. 38, e00703 https://doi.org/10.1016/j.susmat.2023.e00703.
Kusmierek, E., 2020. Semiconductor electrode materials applied in photoelectrocatalytic wastewater treatment - an overview. Catalyst 10 (4), 439. https://doi.org/10.3390/catal10040439.
Li, G., Zhang, Y., Sun, H., An, J., Nie, X., Zhao, H., Wong, P.K., An, T., 2013. Photocatalytic and photoelectrocatalytic degradation of small biological compounds: A case study of uridine. Catal. Today 201, 167–174. https://doi.org/10.1016/j.cattod.2012.03.024.
Li, W., Bai, Y., Zhang, Y., Sun, M., Cheng, R., Xu, X., Chen, Y., Mo, Y., 2005. Effect of hydroxyl radical on the structure of multi-walled carbon nanotubes. Synth. Met. 155 (3), 509–515. https://doi.org/10.1016/j.synthmet.2005.07.346.
Low, J., Yu, J., Jaroniec, M., Wageh, S., Al-Ghamdi, A.A., 2017. Heterojunction Photocatalysts. Adv. Mater. 29 (20), 1601694 https://doi.org/10.1002/adma.201601694.
Martín-Sómer, M., Pablos, C., van Grieken, R., Marugán, J., 2017. Influence of light distribution on the performance of photocatalytic reactors: LED vs mercury lamps. Appl. Catal. B Environ. 215, 1–7. https://doi.org/10.1016/j.apcatb.2017.05.048.
McMichael, S., Fernández-Ibáñez, P., Byrne, J.A., 2021. A review of photoelectrocatalytic reactors for water and wastewater treatment. Water 13 (9), 1198. https://doi.org/10.3390/w13091198.
McMichael, S., Tolosana-Moranchel, A., Cortes, M.A.M., Hamilton, J.W.J., Fernandez-Ibanez, P., Byrne, J.A., 2022. An investigation of photoelectrocatalytic disinfection of water using titania nanotube photoanodes with carbon cathodes and determination of the radicals produced. Appl. Catal. B Environ. 311, 121339 https://doi.org/10.1016/j.apcatb.2022.121339.
Meng, X., Zhang, Z., Li, X., 2015. Synergetic photoelectrocatalytic reactors for environmental remediation: a review. J. Photochem. Photobiol. C. Photochem. Rev. 24, 83–101. https://doi.org/10.1016/j.jphotochemrev.2015.07.003.
Minella, M., Sordello, F., Minero, C., 2017. Photocatalytic process in TiO_2/graphene hybrid materials. Evidence of charge separation by electron transfer from reduced graphene oxide to TiO_2. Catal. Today 281, 29–37. https://doi.org/10.1016/j.cattod.2016.03.040.
Mohamed, R.M., 2012. UV-assisted photocatalytic synthesis of TiO_2-reduced graphene oxide with enhanced photocatalytic activity in decomposition of sarin in gas phase. Desalin. Water Treat. 50 (1–3), 147–156. https://doi.org/10.1080/19443994.2012.708560.
Mohammadi, M., Rezaee Roknabadi, M., Behdani, M., Kompany, A., 2019. Enhancement of visible and UV light photocatalytic activity of rGO-TiO_2 nanocomposites: The effect of TiO_2/Graphene oxide weight ratio. Ceram. Int. 45 (10), 12625–12634. https://doi.org/10.1016/j.ceramint.2019.02.129.
Mondal, A., Prabhakaran, A., Gupta, S., Subramanian, V.R., 2021. Boosting Photocatalytic Activity Using Reduced Graphene Oxide (RGO)/Semiconductor Nanocomposites: Issues and Future Scope. ACS Omega 6 (13), 8734–8743. https://doi.org/10.1021/acsomega.0c06045.
Monteagudo, J.M., Durán, A., San Martín, I., Carrillo, P., 2019. Effect of sodium persulfate as electron acceptor on antipyrine degradation by solar TiO_2 or TiO_2/rGO photocatalysis. Chem. Eng. J. 364, 257–268. https://doi.org/10.1016/j.cej.2019.01.165.
Nakabayashi, Y., Nosaka, Y., 2013. OH Radical Formation at Distinct Faces of Rutile TiO_2 Crystal in the Procedure of Photoelectrochemical Water Oxidation. J. Phys. Chem. C. 117 (45), 23832–23839. https://doi.org/10.1021/jp408244h.
Naknikham, U., Magnacca, G., Qiao, A., Kristensen, P.K., Boffa, V., Yue, Y., 2019. Phenol Abatement by Titanium Dioxide Photocatalysts: Effect of The Graphene Oxide Loading. Nanomaterials 9 (7), 947. https://doi.org/10.3390/nano9070947.
Pablos, C., Marugán, J., Van Grieken, R., Adán, C., Riquelme, A., Palma, J., 2014. Correlation between photoelectrochemical behaviour and photoelectrocatalytic activity and scaling-up of P25-TiO_2 electrodes. Electrochim. Acta 130, 261–270. https://doi.org/10.1016/j.electacta.2014.03.038.
Pastrana-Martínez, L.M., Morales-Torres, S., Likodimos, V., Figueiredo, J.L., Faria, J.L., Falaras, P., Silva, A.M.T., 2012. Advanced nanostructured photocatalysts based on reduced graphene oxide–TiO_2 composites for degradation of diphenhydramine pharmaceutical and methyl orange dye. Appl. Catal. B Environ. 123–124, 241–256. https://doi.org/10.1016/j.apcatb.2012.04.045.
Pei, S., Cheng, H.M., 2011. The reduction of graphene oxide. Carbon 50 (9), 3210–3228. https://doi.org/10.1016/j.carbon.2011.11.010.
Peng, G., Ellis, J.E., Xu, G., Xu, X., Star, A., 2016. In Situ Grown TiO_2 Nanospindles Facilitate the Formation of Holey Reduced Graphene Oxide by Photodegradation. ACS Appl. Mater. Interfaces 8 (11), 7403–7410. https://doi.org/10.1021/acsami.6b01188.
Radich, E.J., Kamat, P.V., 2013. Making Graphene Holey. Gold-Nanoparticle-Mediated Hydroxyl Radical Attack on Reduced Graphene Oxide. ACS Nano 7 (6), 5546–5557. https://doi.org/10.1021/nn401794k.
Rodríguez-Chueca, J., Ormad, M.P., Mosteo, R., Sarasa, J., Ovelleiro, J.L., 2015. Conventional and Advanced Oxidation Processes Used in Disinfection of Treated Urban Wastewater. Water Environ. Res. 87 (3), 281–288. https://doi.org/10.2175/106143014×13987223590362.
Ryu, J., Kim, S., Kim, H., Kim, H.Il., Jo, E.H., Kim, Y.K., Kim, M., Jang, H.D., 2015. Self-assembled TiO_2 agglomerates hybridized with reduced-graphene oxide: A high-performance hybrid photocatalyst for solar energy conversion. Chem. Eng. J. 262, 409–416. https://doi.org/10.1016/j.cej.2014.10.001.
Sanchez Tobon, C., Panžić, I., Bafti, A., Matijašić, G., Ljubas, D., Ćurković, L., 2022. Rapid microwave-assisted synthesis of n/TiO2/rGO nanoparticles for the photocatalytic degradation of pharmaceuticals. Nanomaterials 12 (22), 3975. https://doi.org/10.3390/nano12223975.
Selvaraj, J., Gupta, S., Anand, R., Fiechter, S., Subramanian, V., 2016. How Beneficial Is Reduced Graphene Oxide (RGO) for Long-Term Photo Generated Charge Transport in Bismuth Titanate – RGO Nanocomposite Films? J. Electrochem. Soc. 163 (2), H147–H153. https://doi.org/10.1149/2.0911602jes.
Shams, M., Guiney, L.M., Huang, L., Ramesh, M., Yang, X., Hersam, M.C., Chowdhury, I., 2019. Influence of functional groups on the degradation of graphene oxide nanomaterials. Environ. Sci. Nano. 6 (7), 2203–2214. https://doi.org/10.1039/C9EN00355J.
Song, K., Mohseni, M., Taghipour, F., 2016. Application of ultraviolet light-emitting diodes (UV-LEDs) for water disinfection: A review. Water Res 94 (1), 341–349. https://doi.org/10.1016/j.watres.2016.03.003.
Spilarewicz-Stanek, K., Jakimińska, A., Kisielewska, A., Dudek, M., Piwoński, I., 2021. Graphene oxide photochemical transformations induced by UV irradiation during photocatalytic processes. Mater. Sci. Semicond. Process. 123, 105525 https://doi.org/10.1016/j.mssp.2020.105525.
Taniguchi, T., Wong, K.C., Nurdiwijayanto, L., Hatakeyama, K., Awaya, K., Ida, S., Koinuma, M., Ueda, S., Osada, M., Yokoi, H., 2021. Reversible hydrogenation and irreversible epoxidation induced by graphene oxide electrolysis. Carbon 177, 26–34. https://doi.org/10.1016/j.carbon.2021.02.057.
Tantis, I., Bousiakou, L., Frontistis, Z., Mantzavinos, D., Konstantinou, I., Antonopoulou, M., Karikas, G.A., Lianos, P., 2015. Photocatalytic and photoelectrocatalytic degradation of the drug omeprazole on nanocrystalline titania films in alkaline media: Effect of applied electrical bias on degradation and transformation products. J. Hazard. Mater. 294 (30), 57–63. https://doi.org/10.1016/j.jhazmat.2015.03.042.

Tayebi, M., Kolaei, M., Tayyebi, A., Masoumi, Z., Belbasi, Z., Lee, B.K., 2019. Reduced graphene oxide (RGO) on TiO_2 for an improved photoelectrochemical (PEC) and photocatalytic activity. Sol. Energy 190, 185–194. https://doi.org/10.1016/j.solener.2019.08.020.

Toh, S.Y., Loh, K.S., Kamarudin, S.K., Daud, W.R.W., 2014. Graphene production via electrochemical reduction of graphene oxide: Synthesis and characterisation. Chem. Eng. J. 251, 422–434. https://doi.org/10.1016/j.cej.2014.04.004.

Tolosana-Moranchel, A., Faraldos, M., Bahamonde, A., Pascual, L., Sieland, F., Schneider, J., Dillert, R., Bahnemann, D.W., 2019a. TiO_2-reduced graphene oxide nanocomposites: Microsecond charge carrier kinetics. J. Photochem. Photobiol. A Chem. 386, 112112 https://doi.org/10.1016/j.jphotochem.2019.112112.

Tolosana-Moranchel, A., Manassero, A., Satuf, M.L., Alfano, O.M., Casas, J.A., Bahamonde, A., 2019b. Influence of TiO_2-rGO optical properties on the photocatalytic activity and efficiency to photodegrade an emerging pollutant. Appl. Catal. B Environ. 246, 1–11. https://doi.org/10.1016/j.apcatb.2019.01.054.

Vallejo, W., Rueda, A., Díaz-Uribe, C., Grande, C., Quintana, P., 2019. Photocatalytic activity of graphene oxide–TiO_2 thin films sensitized by natural dyes extracted from Bactris guineensis. R. Soc. Open Sci. 6 (3), 181824 https://doi.org/10.1098/rsos.181824.

Villajos, B., Tolosana-Moranchel, A., Canle, M., Farina, A., Gascó, A., Mesa-Medina, S., Faraldos, M., Hermosilla, D., Bahamonde, A., 2021. Photocatalytic Degradation of Alachlor over Titania-Reduced Graphene Oxide Nanocomposite: Intrinsic Kinetic Model and Reaction Pathways. Ind. Eng. Chem. Res. 60 (51), 18907–18917. https://doi.org/10.1021/acs.iecr.1c04304.

Wang, D., Li, X., Chen, J., Tao, X., 2012. Enhanced photoelectrocatalytic activity of reduced graphene oxide/TiO_2 composite films for dye degradation. Chem. Eng. J. 198–199, 547–554 https://doi.org/10.1016/j.cej.2012.04.062.

Wang, P., Ao, Y., Wang, C., Hou, J., Qian, J., 2012. Enhanced photoelectrocatalytic activity for dye degradation by graphene–titania composite film electrodes. J. Hazard. Mater. 223–224, 9–83. https://doi.org/10.1016/j.jhazmat.2012.04.050.

Wang, Y., Zu, M., Zhou, X., Lin, H., Peng, F., Zhang, S., 2020. Designing efficient TiO_2-based photoelectrocatalysis systems for chemical engineering and sensing. Chem. Eng. J. 381, 122605 https://doi.org/10.1016/j.cej.2019.122605.

Waso, M., Khan, S., Singh, A., McMichael, S., Ahmed, W., Fernández-Ibáñez, P., Byrne, J. A., Khan, W., 2020. Predatory bacteria in combination with solar disinfection and solar photocatalysis for the treatment of rainwater. Water Res 169, 115281. https://doi.org/10.1016/j.watres.2019.115281.

Xu, L., Cheng, L., 2013. Graphite Oxide under High Pressure: A Raman Spectroscopic Study. J. Nanomater. 2013, 1–5. https://doi.org/10.1155/2013/731875.

Žerjav, G., Arshad, M.S., Djinović, P., Junkar, I., Kovač, J., Zavašnik, J., Pintar, A., 2017. Improved electron–hole separation and migration in anatase TiO_2 nanorod/reduced graphene oxide composites and their influence on photocatalytic performance. Nanoscale 9 (13), 4578–4592. https://doi.org/10.1039/C7NR00704C.

Zhou, X., Zhang, Y., Wang, C., Yang, Y., Zheng, B., Wu, H., Guo, S., Zhang, J., 2012. Photo-Fenton Reaction of Graphene Oxide: A New Strategy to Prepare Graphene Quantum Dots for DNA Cleavage. ACS Nano 6 (8), 6592–6599. https://doi.org/10.1021/nn301629v.

Zuo, J., Yuan, S., Li, Y., Tan, C., Xia, Z., Yang, S., Yu, S., Li, J., 2021. RSM-Based Preparation and Photoelectrocatalytic Performance Study of RGO/TiO_2 NTs Photoelectrode. Processes 9 (9), 1492. https://doi.org/10.3390/pr9091492.